

Constraints on Massive Neutrinos from the CFHTLS Angular Power Spectrum

Jun-Qing Xia¹, Benjamin R. Granett², Matteo Viel^{3,4}, Simeon Bird⁵, Luigi Guzzo²,
Martin G. Haehnelt⁶, Jean Coupon⁷, Henry Joy McCracken⁸, and Yannick Mellier⁸

¹*Scuola Internazionale Superiore di Studi Avanzati, Via Bonomea 265, I-34136 Trieste, Italy*

²*INAF-Osservatorio Astronomico di Brera, Via E. Bianchi 46, 23807, Italy*

³*INAF-Osservatorio Astronomico di Trieste, Via G.B. Tiepolo 11, I-34131 Trieste, Italy*

⁴*INFN/National Institute for Nuclear Physics, Via Valerio 2, I-34127 Trieste, Italy*

⁵*School of Natural Sciences, Institute for Advanced Study, Princeton, NJ 08540, USA*

⁶*Institute of Astronomy and Kavli Institute for Cosmology,*

Madingley Road, CB3 0HA, Cambridge, United Kingdom

⁷*Institute of Astronomy and Astrophysics, Academia Sinica, P.O. Box 23-141, Taipei 10617, Taiwan and*

⁸*Institut d'Astrophysique de Paris, UMR 7095 CNRS,*

Université Pierre et Marie Curie, 98 bis Boulevard Arago, 75014 Paris, France

(Dated: July 13, 2018)

We use the galaxy angular power spectrum at $z \sim 0.5 - 1.2$ from the Canada-France-Hawaii-Telescope Legacy Survey Wide fields (CFHTLS-Wide) to constrain separately the total neutrino mass $\sum m_\nu$ and the effective number of neutrino species N_{eff} . This survey has recently benefited from an accurate calibration of the redshift distribution, allowing new measurements of the (non-linear) matter power spectrum in a unique range of scales and redshifts sensitive to neutrino free streaming. Our analysis makes use of a recent model for the effect of neutrinos on the weakly non-linear matter power spectrum derived from accurate N-body simulations. We show that CFHTLS, combined with WMAP7 and a prior on the Hubble constant provides an upper limit of $\sum m_\nu < 0.29$ eV and $N_{\text{eff}} = 4.17_{-1.26}^{+1.62}$ (2σ confidence levels). If we omit smaller scales which may be affected by non-linearities, these constraints become $\sum m_\nu < 0.41$ eV and $N_{\text{eff}} = 3.98_{-1.20}^{+2.02}$ (2σ confidence levels). Finally we show that the addition of other large scale structures probes can further improve these constraints, demonstrating that high redshift large volumes surveys such as CFHTLS are complementary to other cosmological probes of the neutrino mass.

I. INTRODUCTION

Determining the neutrino mass is one of the great unsolved problems of modern particle physics. The standard model contains three massless neutrino species; observations of neutrino oscillations in atmospheric and solar neutrino experiments have confirmed that neutrinos are massive, but cannot pin down their absolute mass scale. Fortunately, the Universe offers a new laboratory for neutrino physics. Massive neutrinos affect both the background expansion and the growth of cosmological structure, making cosmological observations an unrivaled probe of the total neutrino mass [1, 2].

The redshift at which massive neutrinos become non-relativistic alters the time since matter-radiation equality, thus changing the position of the Cosmic Microwave Background (CMB) anisotropy peaks. Measurements of the CMB have used this effect to find $\sum m_\nu < 1.3$ eV (95% C.L.) [3–6], and a sensitivity of $\sigma(\sum m_\nu) \sim 0.3$ eV could soon be achieved with the Planck satellite (e.g. [2]).

Massive neutrinos also play a role in the formation of large scale structure. Once non-relativistic, they damp the growth of perturbations within their free streaming scale, resulting in a suppression of the small-scale linear matter power spectrum of $\Delta P/P \sim -8\Omega_\nu/\Omega_m$ [7]. Measurements of the matter power spectrum can thus improve constraints on the neutrino mass considerably. Many analyses have been performed combining CMB data with Large Scale Structure (LSS) probes such as the 2dF Galaxy Redshift Survey (2dFGRS) [8–10], the Sloan Digital Sky Survey (SDSS) [11–24], WiggleZ [25] and the SDSS Lyman- α forest [26–28] to constrain $\sum m_\nu$. The combination of the SDSS DR8 LRG angular power spectra, WMAP7 data and an HST prior on the Hubble constant gives $\sum m_\nu < 0.26$ eV (95% C.L.), assuming a flat Λ CDM model with the standard model effective number of neutrino species, $N_{\text{eff}} = 3.04$ [29, 30].

A detection of $N_{\text{eff}} > 3.04$, as recently hinted at by the Atacama Cosmology Telescope (ACT) and the South Pole Telescope (SPT) experiments [31, 32], would imply additional relativistic relics or non-standard neutrino properties. The additional energy density of extra relativistic particle species would change the redshift of matter-radiation equality, leaving imprints on the CMB anisotropies and matter power spectrum. Parameter degeneracies limit the constraining power of the primary CMB anisotropies on N_{eff} [4, 5, 33]. The 95% lower limit is $N_{\text{eff}} > 2.7$ from WMAP7 alone [6]. Adding information on the matter power spectrum and the Hubble constant can tighten the constraint significantly [21, 23, 32, 34–37], as can measurements of smaller scale CMB fluctuations.

In this work, we introduce new constraints from measurements of the angular power spectrum of galaxies at

$z \sim 0.5 - 1.2$ in the Canada-France-Hawaii-Telescope Legacy Survey Wide fields (CFHTLS-Wide) [38]. This is the deepest wide-field survey of its kind, covering 133 sq. deg. and sampling a comoving volume of $0.2 \text{ Gpc}^3/h^3$ from $z = 0.5 - 1.2$. This data has been used for cosmological studies, including weak lensing constraints [39–42]. In particular, a joint analysis using the weak lensing measurements has given a limit for massive neutrinos of $\sum m_\nu < 0.54 \text{ eV}$ (95% C.L.) [43]. The small-scale clustering was studied using the halo model by ref. [44] and the deprojected power spectrum was presented in ref. [45].

Considerable gains can be made by probing the power spectrum on weakly non-linear scales, provided one can model the galaxy bias sufficiently accurately. On large scales, the galaxy power spectrum is well-fit by the dark matter power spectrum and a linear galaxy bias: $\delta_g = b_g \delta_{dm}$. On small scales, where the details of galaxy formation come into play, this relation breaks down and a general, scale-dependent, galaxy bias model is necessary [46–48]. This results in a degeneracy between galaxy bias and cosmological parameters that is difficult to break without further observations such as gravitational lensing [49].

The scale-dependence of galaxy clustering has been investigated with simulations [46, 50] and observations [47]. These studies show that galaxies with lower luminosity have a weaker scale-dependence of the bias than the most luminous ones at $k > 0.1 \text{ h/Mpc}$. Additionally, the scale dependence becomes more severe for strongly biased tracers; negligible scale dependence of the halo bias is found in simulations at $k = 0.15 \text{ h/Mpc}$ for halos with $b_g < 2$, while for more massive halos with $b_g > 2$, there is a 20% effect [50]. For the SDSS main sample, the `Halofit` non-linear matter power spectrum with a constant bias factor has been demonstrated to be a good fit to the galaxy power spectrum [51], while the power spectrum of the LRG sample diverges at $k = 0.2 \text{ h/Mpc}$ [48].

We select the range of scales to study based on the dominance of the two-halo term in the halo occupation distribution (HOD) model of the power spectrum. In ref. [44], HOD fits are made to the correlation function of the CFHTLS galaxies. We have checked explicitly that the two-halo term is greater than the one-halo term to $\ell = 960$ in our lowest redshift sample ($0.5 < z_{\text{phot}} < 0.6$). In Sec. V we test our CFHTLS data set using a comparison of the constant bias model with a two-parameter model in the context of ΛCDM without massive neutrinos. We conclude that a constant bias model is sufficient.

The CFHTLS data set is ideal for this study because (i) at higher redshift the onset of non-linear growth happens at smaller scales; and (ii) we are targeting “normal” galaxies: the flux limited sample that we construct ($i_{\text{AB}} < 22.5$) selects galaxies to $z = 1$ with luminosities of $M_g \sim -20$, similar to the SDSS main sample at $z = 0.1$ [52, 53].

Since we analyze the projected density field, any modulation of the power spectrum due to redshift-space distortions is minimized, although these effects must be considered for surveys covering a larger fraction of the sky than CFHTLS [19]. We must also consider systematic errors arising from the luminosity dependence of the galaxy bias. In a flux-limited sample with a mixture of galaxy types, luminosity-dependent biasing can modify the slope of the galaxy power spectrum. However, for current surveys such as 2dFGRS, the effects can be neglected [54].

In this paper we will present constraints on the total mass of neutrinos, $\sum m_\nu$, and the effective number of neutrino species, N_{eff} , from different cosmological observations. The structure of the paper is as follows: In section II we briefly review the general formalism of the angular power spectrum C_ℓ . In sections III and IV we describe the recently released CFHTLS clustering power spectra data set, and the other data sets we use. Section V contains our main results on $\sum m_\nu$ and N_{eff} , while section VI is dedicated to the conclusions and discussion.

II. ANGULAR POWER SPECTRUM

The angular power spectrum, C_ℓ , is a projection of the spatial power spectrum of fluctuations, $P_{\text{gal}}(k, z)$, where k is the comoving wave number and z is the redshift. The equation for the projection is

$$C_\ell = \frac{2b^2}{\pi} \int k^2 dk P(k) g_\ell^2(k), \quad (1)$$

where $P(k)$ is the matter power spectrum today and b is the assumed scale-independent bias factor relating the galaxy overdensity to the mass overdensity. In our calculations, we assume the values of bias are constant in each redshift bin; with width $\Delta z \sim 0.2$, these are relatively narrow. We also neglect the effect of redshift space distortions, as their effect is limited to large scales, $\ell < 30$ [55], and our largest bin is at $\ell = 40$. With these assumptions, the kernel $g_\ell(k)$ is given by

$$g_\ell(k) = \int_{z_{\text{min}}}^{z_{\text{max}}} dz D(z) j_\ell(k\chi(z)) \frac{dN}{dz}(z) \left[\frac{dz}{d\chi}(z) \right], \quad (2)$$

where $j_\ell(x)$ is the spherical Bessel function, $\chi(z)$ is the comoving distance to redshift z , and $dN/dz(z)$ is the normalized redshift distribution of the survey.

The Limber approximation is valid for all but the largest angular scales ($\ell \gtrsim 10$). For $\ell \gg 1$, we have

$$\frac{2}{\pi} \int k^2 dk j_\ell(k\chi) j_\ell(k\chi') = \frac{1}{\chi^2} \delta(\chi - \chi'), \quad (3)$$

and the equation for the projection becomes

$$C_\ell = b^2 \int_{z_{\min}}^{z_{\max}} P\left(k = \frac{\ell + 1/2}{\chi(z)}, z\right) \left[\frac{dN}{dz}(z)\right]^2 \frac{dz}{dV_c(z)}, \quad (4)$$

where $dV_c(z)$ is the comoving volume element, $dV_c(z) = \chi^2 d\chi/dz$.

III. C_ℓ MEASUREMENTS OF CFHTLS

A. Data

We analyze the galaxy density maps constructed by ref. [45] from the Canada-France-Hawaii Legacy Survey Wide fields (CFHTLS-Wide). The data set is based on the CFHTLS T0006 release, including photometric redshift estimates [52]. A selection of galaxies was made photometrically to an apparent flux limit of $i_{AB} = 22.5$ in three photometric redshift bins: $0.5 - 0.6$, $0.6 - 0.8$, and $0.8 - 1.0$, labeled S6, S7 and S8. We are not overly concerned with the error in the photometric redshift estimates, although it is typically $\Delta z/(1+z) = 0.04$ [52]; we only require knowledge of the redshift distributions of the samples. In ref. [45], the redshift distributions were measured using a subset of ~ 14000 spectroscopic redshifts obtained from the VIMOS Public Extragalactic Redshift Survey (VIPERS) [56]. We also use those redshift distributions here.

B. C_ℓ estimator

We estimate the C_ℓ with a maximum likelihood approach first applied to cosmic microwave background maps [57, 58]. It is well suited to fields that may be described by a Gaussian likelihood function, and it has been extended successfully to measure the angular power spectrum in galaxy surveys [59, 60].

For surveys that cover only a relatively small patch of sky, such as CFHTLS, the maximum likelihood approach has advantages over other techniques. Generally, it is challenging to measure harmonic modes that are strongly affected by the survey geometry. Modes become correlated due to the convolution effect of the survey mask; further, the hard edges can introduce ‘ringing’ in harmonic space. Our estimator accounts for these effects and measures the C_ℓ with minimum variance (in the case of a Gaussian field). Along with the C_ℓ , we derive the covariance matrix of the measurements and window functions.

The galaxy density maps were constructed on a HEALPix¹ grid with an angular resolution of 7 arcmin ($n_{\text{side}} = 512$) [61]. We order the m pixels of the density map, form a data vector, $\mathbf{x} = [\delta(\hat{\mathbf{n}}_0), \delta(\hat{\mathbf{n}}_1), \dots, \delta(\hat{\mathbf{n}}_{m-1})]$, and write the covariance of the data as $C_{ij} = \langle x_i x_j \rangle$. The pixel covariance matrix is given by the sum of the signal and the noise components

$$C_{ij} = \sum_l \frac{2l+1}{4\pi} \mathcal{P}_l(\cos \theta_{ij}) B_l^2 C_\ell + N_{ij}, \quad (5)$$

where \mathcal{P}_ℓ are the Legendre polynomials, θ_{ij} is the separation between pixels i and j and N_{ij} is the noise covariance matrix. The noise matrix is taken to be diagonal with Poisson elements given by $N_{ii} = w_i^2/\bar{n}$, where w_i is a weight accounting for partially-sampled pixels. The finite resolution of the pixelized map attenuates the power spectrum by the pixel window function, B_ℓ , which depends on the pixel geometry [61].

To simplify the following expressions, we introduce a symmetric matrix \mathbf{P}_b . This is a sum of the Legendre polynomials over a band-power indexed by b including $[\ell_b, \ell_{b+1})$. The components are

$$P_{b,ij} = \sum_{\ell_b \leq \ell < \ell_{b+1}} \frac{2\ell+1}{4\pi} \mathcal{P}_\ell(\cos \theta_{ij}) B_\ell^2, \quad (6)$$

¹ <http://healpix.jpl.nasa.gov>

TABLE I: CFHTLS samples

Photo-z sample		\bar{z}	Scale (h/Mpc)	
			$\ell = 630$	$\ell = 960$
S6	$0.5 < z_{\text{phot}} < 0.6$	0.557	0.43	0.65
S7	$0.6 < z_{\text{phot}} < 0.8$	0.687	0.36	0.55
S8	$0.8 < z_{\text{phot}} < 1.0$	0.839	0.31	0.47

The quadratic band-power estimator is given by

$$\hat{C}_b = \frac{1}{2} \sum_j A_{ij} \{ \mathbf{x}^T \mathbf{C}^{-1} \mathbf{P}_b \mathbf{C}^{-1} \mathbf{x} - \text{Tr}(\mathbf{C}^{-1} \mathbf{P}_b \mathbf{C}^{-1} \mathbf{N}) \}. \quad (7)$$

The matrix \mathbf{A} is a mixing matrix that sets the normalization and may be specified to form linear combinations of the bin estimates. It is related to the Fisher matrix,

$$F_{bb'} = \frac{1}{2} \text{Tr}(\mathbf{C}^{-1} \mathbf{P}_b \mathbf{C}^{-1} \mathbf{P}_{b'}). \quad (8)$$

The expectation and variance of the estimator are

$$\langle \hat{\lambda} \rangle = \mathbf{A} \mathbf{F} \lambda, \quad (9)$$

$$\text{Var}(\hat{\lambda}, \hat{\lambda}) = \mathbf{A} \mathbf{F} \mathbf{A}^T, \quad (10)$$

and the window functions are $\mathbf{W} = \mathbf{A} \mathbf{F}$. The matrix \mathbf{A} can be chosen in a variety of ways to optimize the estimator [57]. Because the Fisher matrix is ill-conditioned due to the small survey size, we use the robust normalization $A_{ii} = (\sum_j F_{ij})^{-1}$.

The covariance between the C_ℓ measurements of two redshift slices labeled A and B may be estimated as

$$\text{Var}(C_\ell^A, C_\ell^B) = \frac{1}{f_{sky}} \frac{2}{2\ell + 1} (C_\ell^{AB})^2, \quad (11)$$

where C_ℓ^{AB} is given by eq. (1), rewriting as

$$C_\ell^{AB} = \frac{2b_A b_B}{\pi} \int k^2 dk P(k) g_\ell^A(k) g_\ell^B(k). \quad (12)$$

We must further convolve by the survey window functions. This is an idealization that neglects the precise survey geometry but we may scale it to match the variance computed from the quadratic estimator

C. C_ℓ measurements

The quadratic C_ℓ estimator operates under the assumption that the galaxy density can be described by a Gaussian random field, which is not valid on small scales. However, Gaussianity can be a reasonable model for galaxy counts in projection even to non-linear scales. Our map resolution is 7 arcmin/pixel ($n_{\text{side}} = 512$) and, in the first redshift bin, S6, the mean and median counts are 33.6 and 32.0 galaxies/pixel, respectively, with skewness 1.18. At a higher resolution of 3.5 arcmin/pixel, the mean and median become 8.42 and 7.72 with skewness 1.48. We see that the map resolution of 7 arcmin/pixel gives a good balance between Gaussianity and angular scale. We expect that the Gaussianity assumption is still valid at scales typical of the pixel size at $\ell = 1500$.

We compute the angular power spectrum in 48 bins over the range $\ell = 2 - 960$, with width $\Delta\ell = 20$. The Fisher matrix and window functions were computed with step size $\Delta\ell = 10$. Due to the small angular extent of the survey, we cannot probe low ℓ and, indeed, the computed window functions show that we are not sensitive to $\ell < 40$.

We estimate C_ℓ for the three photometric samples, S6, S7 and S8. The measurements are shown in figure 1. The Fourier scales that are probed in the angular power spectrum depend on the projection kernel g_ℓ . In figure 2, we plot representative kernels. We use two limits in angular scale in the subsequent cosmological analysis: $\ell_{\text{max}} = 630$ and $\ell_{\text{max}} = 960$.

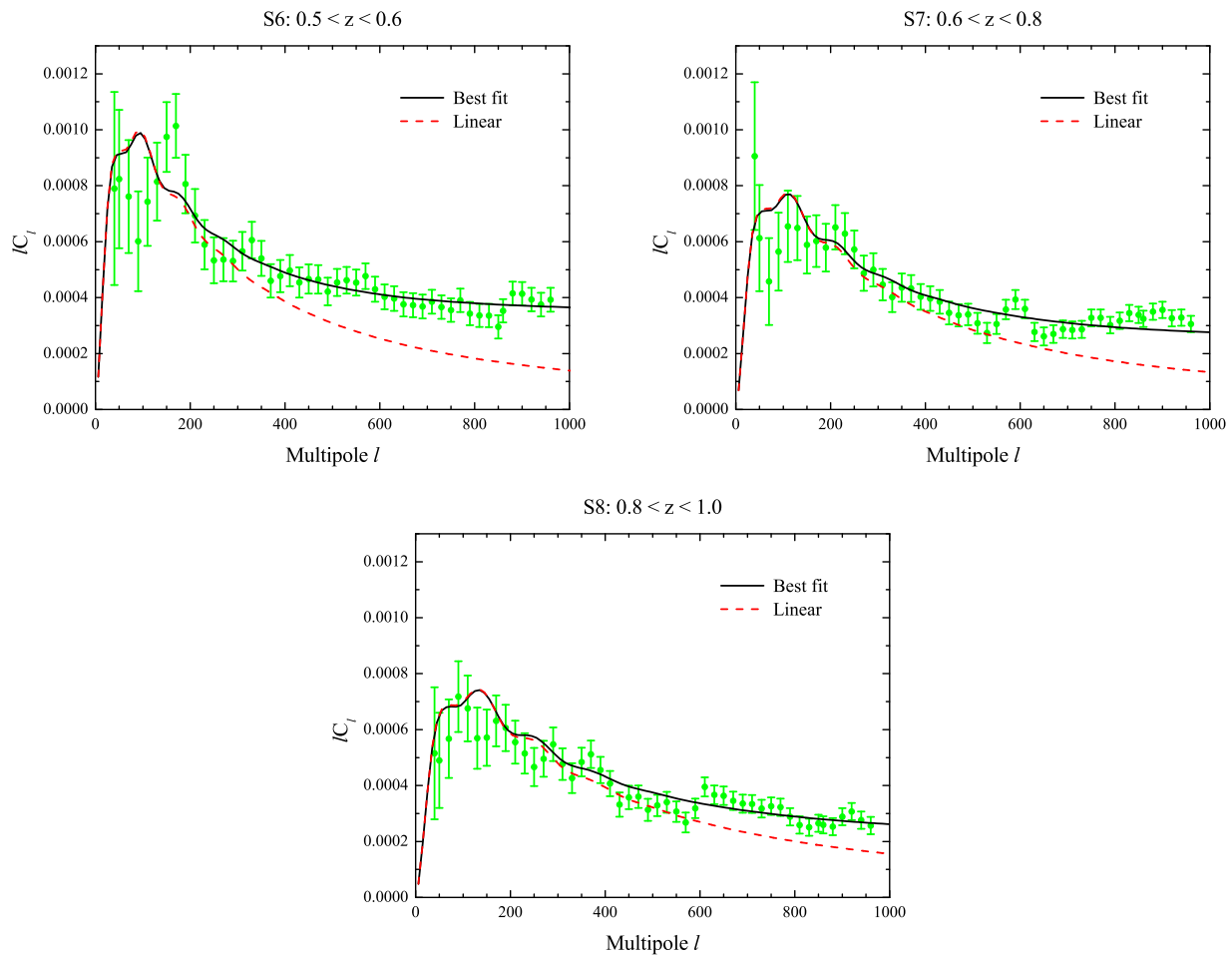


FIG. 1: The angular power spectra for the three different redshift bins. We show the data with 1σ error bars and the linear (dashed curves) and non-linear (continuous curves) theoretical angular power spectra.

IV. EXTERNAL DATA SETS

Besides the angular power spectra C_ℓ of the CFHTLS measurement, we will also consider the following cosmological probes: i) power spectra of CMB temperature and polarization anisotropies; ii) power spectra of luminous red galaxies; iii) measurement of the current Hubble constant; iv) luminosity distances of type Ia supernovae. These data sets are all well established cosmological probes that have been extensively investigated and already provide tight constraints on the cosmological parameters of the concordance Λ CDM model we will use here.

A. CMB Power Spectra Data

To incorporate the seven-year WMAP (WMAP7) CMB temperature and polarization power spectra, we use the routines for computing the likelihood supplied by the WMAP team [6]. The WMAP7 polarization data are composed of TE/EE/BB power spectra on large scales ($2 \leq \ell \leq 23$) and TE power spectra on small scales ($24 \leq \ell \leq 800$), while the WMAP7 temperature data includes the CMB anisotropies on scales $2 \leq \ell \leq 1200$.

Here we do not use other small-scale CMB temperature power spectra measurements, as adding them would not significantly improve the constraints on the cosmological parameters, especially those on the total neutrino mass focussed on in this paper.

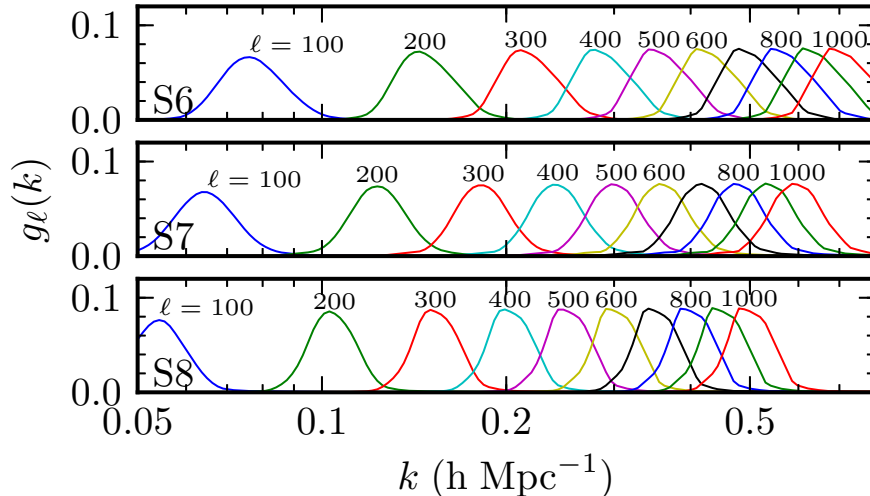


FIG. 2: The projection kernels $g_\ell(k)$ defined in eq. (2) for the three CFHTLS samples S6, S7 and S8 with mean redshifts 0.557, 0.687 and 0.839. The normalized kernels are plotted.

B. Power Spectrum of Luminous Red Galaxies

The power spectrum of LRGs measured by SDSS is a powerful probe of the total mass of neutrinos, $\sum m_\nu$, and the effective number of neutrino species, N_{eff} . We thus include the SDSS DR4 LRG power spectrum [62] which has a mean redshift $\bar{z} \sim 0.35$ and use data points on scales $0.012 h/\text{Mpc} < k_{\text{eff}} < 0.203 h/\text{Mpc}$ in the analysis.

We checked the constraining power of the SDSS DR7 LRG power spectrum [21] and found that the constraint on the total neutrino mass does not improve significantly. For simplicity, we still use the SDSS DR4 LRG power spectrum [62]. Furthermore, we do not include the BAO information [22], as the measurement of BAO and LRGs power spectrum cannot be treated as independent data sets.

C. Hubble Constant

In our analysis, we add a Gaussian prior on the current Hubble constant given by ref. [63]; $H_0 = 74.2 \pm 3.6 \text{ km s}^{-1} \text{ Mpc}^{-1}$ (68% C.L.). The quoted error includes both statistical and systematic errors. This measurement of H_0 is obtained from the magnitude-redshift relation of 240 low- z Type Ia supernovae at $z < 0.1$ by the Near Infrared Camera and Multi-Object Spectrometer (NICMOS) Camera 2 of the Hubble Space Telescope (HST). This is a significant improvement over the previous prior, $H_0 = 72 \pm 8 \text{ km s}^{-1} \text{ Mpc}^{-1}$, which is from the Hubble Key project final result [64]. In addition, we impose a weak top-hat prior on the Hubble parameter: $H_0 \in [40, 100] \text{ km s}^{-1} \text{ Mpc}^{-1}$.

D. Luminosity Distances

Finally, we include data from Type Ia supernovae, which consists of luminosity distance measurements as a function of redshift; $D_L(z)$. In this paper we use the latest SNIa data sets from the Supernova Cosmology Project, “Union Compilation 2.1”, which consists of 580 samples and spans the redshift range $0 \lesssim z \lesssim 1.55$ [65]. This data set also provides the covariance matrix of data with and without systematic errors. In order to be conservative, we use the covariance matrix with systematic errors. When calculating the likelihood from SNIa, we marginalize over the absolute magnitude M , which is a nuisance parameter, as done in refs. [66, 67].

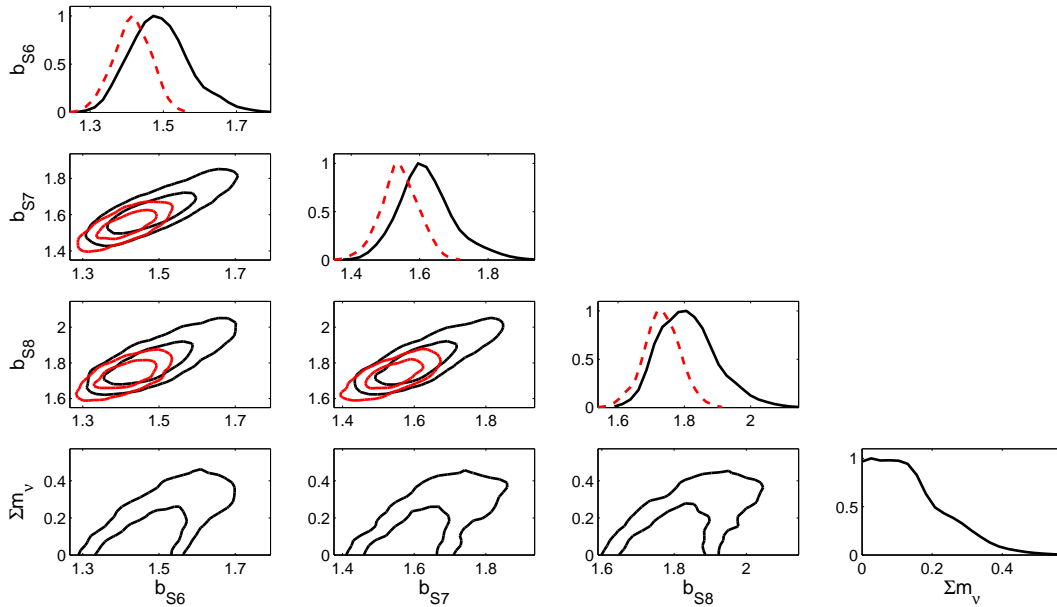


FIG. 3: Marginalized one-dimensional and two-dimensional likelihood ($1, 2\sigma$ contours) constraints on the total neutrino mass and the three CFHTLS bias parameters from WMAP7+HST+SDSS+SN+CFHTLS data combination for $\ell_{\max} = 630$. We also show the constraints on the bias parameters, assuming massless neutrinos (red dashed lines).

V. NUMERICAL RESULTS

We model the nonlinear matter power spectrum $P(k)$ using the `Halofit` formulae [68] as modified to account for massive neutrinos [69]. This modified version of `Halofit` was obtained from an extensive suite of N-body simulations which treat massive neutrinos as an independent set of particles [70], and was particularly focused on exploring small scales at redshifts $z = 0 - 2$. Similar simulations have been used to estimate the redshift space distortions and bias between matter and haloes [71].

We perform a global fitting of cosmological parameters using the `CosmoMC` package [72], a Markov Chain Monte Carlo (MCMC) code. We assume purely adiabatic initial conditions and a flat Λ CDM Universe, with no tensor contribution to primordial fluctuations. The following six cosmological parameters are allowed to vary with top-hat priors: the dark matter energy density parameter $\Omega_c h^2 \in [0.01, 0.99]$, the baryon energy density parameter $\Omega_b h^2 \in [0.005, 0.1]$, the primordial spectral index $n_s \in [0.5, 1.5]$, the primordial amplitude $\log[10^{10} A_s] \in [2.7, 4.0]$, the ratio (multiplied by 100) of the sound horizon at decoupling to the angular diameter distance to the last scattering surface $\Theta_s \in [0.5, 10]$, and the optical depth to reionization $\tau \in [0.01, 0.8]$. The pivot scale is set at $k_{s0} = 0.05 \text{ Mpc}^{-1}$. Besides these six basic cosmological parameters, we pay particularly attention to the neutrino mass fraction at the present day

$$f_\nu \equiv \frac{\Omega_\nu h^2}{\Omega_m h^2} = \frac{\sum m_\nu}{93.14 \text{ eV } \Omega_m h^2}, \quad (13)$$

the effective number of neutrino species, N_{eff} , and the three CFHTLS galaxy bias parameters, b_{S6} , b_{S7} , b_{S8} . Note that in our analyses we do not vary $\sum m_\nu$ and N_{eff} simultaneously, since they are no longer degenerate [73]. Instead, we assume $N_{\text{eff}} = 3.04$ to constrain the total mass of neutrinos and $\sum m_\nu = 0$ to constrain N_{eff} .

A. CFHTLS galaxy bias

We first measure the galaxy bias in the context of the Λ CDM model, without introducing massive neutrinos. We find the 68% C.L. constraints on the bias parameters to be: $b_{S6} = 1.41 \pm 0.05$, $b_{S7} = 1.54 \pm 0.05$ and $b_{S8} = 1.73 \pm 0.06$, which are in good agreement with those derived by ref. [45]. The bias values are consistent, but higher than those found by ref. [44] for volume limited samples in CFHTLS covering the same redshift ranges. This discrepancy could

TABLE II: The 95% confidence level upper limits on the total mass of neutrinos $\sum m_\nu$ from different data combinations.

95% C.L. $\sum m_\nu$ [eV]	Without HST Prior		With HST Prior	
	$\ell_{\max} = 630$	$\ell_{\max} = 960$	$\ell_{\max} = 630$	$\ell_{\max} = 960$
WMAP7	1.17		0.50	
WMAP7 + CFHTLS	0.64	0.43	0.41	0.29
WMAP7 + SDSS + CFHTLS	0.47	0.35	0.35	0.28
WMAP7 + SDSS + SN + CFHTLS	–	–	0.33	0.27

arise from differences in the analysis method; in ref. [44], the cosmology was fixed and the fit was carried out over halo model parameters using the correlation function on small scales ($< 1^\circ$). Generally, the best-fitting bias values are correlated with the other parameters considered in the analysis. In particular, we will find that they shift when we introduce massive neutrinos.

We also check whether a scale-dependent bias is supported by the data, again assuming Λ CDM without massive neutrinos. We compute the best-fitting parameters assuming a scale-dependent Q bias model [74] with the form

$$b(k) = b_{\text{lin}} \sqrt{\frac{1 + Qk^2}{1 + Ak}}. \quad (14)$$

We fix the parameter $A = 1.7 \text{ Mpc/h}$ and find the best-fitting Q .

We first perform the fit using the linear power spectrum, such that $P(k) = b^2(k)P_{\text{lin}}(k)$. The best-fitting Q value is $Q_{\text{lin}} = 10.3 \pm 1.5$. If we instead use a non-linear `Halofit` power spectrum (without massive neutrinos), the best-fitting Q value is reduced to $Q_{\text{halofit}} = 2.5 \pm 1.2$ and scale dependence in the bias at the $< 5\%$ level at $k < 0.6 \text{ h/Mpc}$, which is negligible. The robust fit using `Halofit` and a simple constant bias is expected, since the data is well-fit by the two-halo clustering term on these scales [44]. This demonstrates that the assumption of constant galaxy bias is a good one, and our results for massive neutrinos are robust.

Before presenting the constraints on the total neutrino mass, we examine the degeneracies between the total neutrino mass and the three CFHTLS bias parameters. In figure 3 we show the marginalized one-dimensional and two-dimensional likelihood constraints from the WMAP7+HST+SDSS+SN+CFHTLS data combination. The black solid lines and the red dashed lines denote the constraints with massless and massive neutrinos, respectively. When including massive neutrinos, the constraints on the bias parameters are obviously weakened and the median values are shifted: $b_{S6} = 1.49 \pm 0.07$, $b_{S7} = 1.62 \pm 0.08$ and $b_{S8} = 1.81 \pm 0.08$ (68% C.L.). This results in a strong correlation between $\sum m_\nu$ and the bias parameters; clearly shown in the two-dimensional contours of the last row of figure 3. A larger total neutrino mass will suppress the amplitude of the matter power spectrum on small scales further. Countering this while still matching the CFHTLS data on small scales requires larger bias parameters. Thus, further improving the constraints on the total neutrino mass will require better determination of the bias parameters.

B. Neutrino Mass $\sum m_\nu$

In this subsection, we present the 95% confidence level upper limits on the total mass of neutrinos from different data combinations after marginalizing over the other parameters, as shown in table II.

We start by presenting the limits using scales up to $\ell_{\max} = 630$. Due to the strong degeneracies present between cosmological parameters, primary CMB anisotropies alone can place only weak constraints on the total neutrino mass. In the flat Λ CDM framework, WMAP7 alone constrains $\sum m_\nu < 1.17 \text{ eV}$ at the 95% confidence level [6]. Adding the low redshift CFHTLS measurements breaks these degeneracies and the constraint on the total neutrino mass significantly improves to

$$\sum m_\nu < 0.64 \text{ eV} \quad (95\% \text{ C.L.}) \quad (15)$$

for the combined WMAP7 and CFHTLS datasets. In figure 4, we plot the one-dimensional marginalized distributions on some cosmological parameters from different data combinations. As can be seen, adding CFHTLS data improves the constraints on the present matter density Ω_m , the amplitude of fluctuations σ_8 and the hubble parameter H_0 ; their 68% confidence levels are shrunk from 0.334 ± 0.053 , 0.711 ± 0.062 and 65.1 ± 3.7 for WMAP7 alone to 0.320 ± 0.043 , 0.759 ± 0.044 and 66.3 ± 3.1 for WMAP7+CFHTLS data, respectively. In figure 5 we show the two-dimensional contours in the $(\sigma_8, \sum m_\nu)$, $(\Omega_m, \sum m_\nu)$ and $(H_0, \sum m_\nu)$ planes from different data combinations. Using WMAP7+CFHTLS

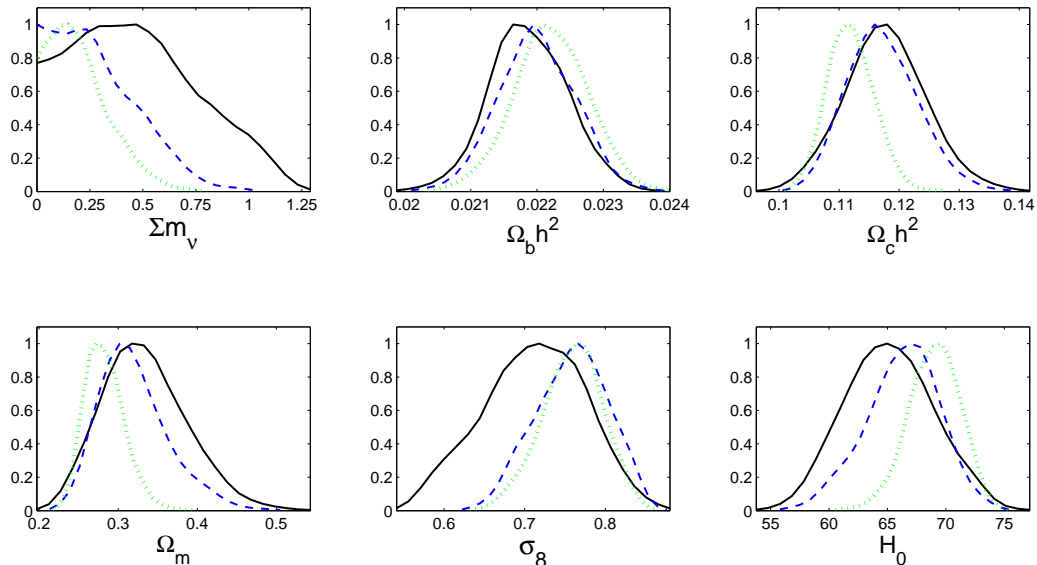


FIG. 4: One-dimensional marginalized likelihood constraints on the total neutrino mass $\sum m_\nu$, as well as other cosmological parameters, $\Omega_b h^2$, $\Omega_c h^2$, Ω_m , σ_8 and H_0 from different data combinations: WMAP7 alone (black solid lines), WMAP7+CFHTLS (blue dashed lines) and WMAP7+SDSS+CFHTLS (green dotted lines) for $\ell_{\max} = 630$.

data (blue dashed lines) reduces the correlations between $\sum m_\nu$ and other parameters and gives tighter constraints on $\sum m_\nu$ than WMAP7 alone (black solid lines).

Using the SDSS DR4 LRG power spectrum data [62], we obtain a constraint on the total neutrino mass of $\sum m_\nu < 0.62$ eV at the 95% confidence level, comparable to the limit from WMAP7+CFHTLS. For comparison, we also use the SDSS DR7 LRG power spectra data [21] to constrain $\sum m_\nu$ and get a 95% C.L. upper limit of $\sum m_\nu < 0.61$ eV, which is almost identical with that from DR4 LRG data. Due to this negligible improvement, in our calculations we still use the SDSS DR4 data to avoid using the more complicated DR7 likelihood code. Figure 4 (green dashed lines) clearly shows that the constraints on Ω_m , σ_8 and H_0 are much tighter when including the SDSS data set. We obtain a constraint on the total neutrino mass of $\sum m_\nu < 0.47$ eV at the 95% confidence level from the combination of WMAP7+SDSS+CFHTLS data.

We next consider the constraints using WMAP7 with an HST prior. The degeneracy between H_0 and $\sum m_\nu$, clearly shown in figure 5, means that independent measurements of H_0 produce significantly tighter overall constraints. WMAP7+HST gives the 95% C.L. upper limit $\sum m_\nu < 0.50$ eV. After adding the low redshift CFHTLS clustering power spectra data, the constraint becomes even tighter

$$\sum m_\nu < 0.41 \text{ eV} \quad (95\% \text{ C.L.}) . \quad (16)$$

In figure 6 we show the one-dimensional marginalized distributions on some cosmological parameters from different data combinations when the HST prior is used. Clearly, the CFHTLS data improves the constraints on some cosmological parameters, reducing the correlations between them and $\sum m_\nu$ further, and thus significantly improving the limit on $\sum m_\nu$.

For comparison, we use the SDSS DR4 LRG power spectra data to constrain $\sum m_\nu$ and obtain the 95% upper limit 0.45 eV, comparable to that from the CFHTLS data set. Similarly, we use the SDSS DR7 LRG data and obtain the constraint $\sum m_\nu < 0.43$ eV (95% C.L.), which is consistent with previous work [6]. When using SDSS and CFHTLS data sets together, we get tighter constraints on the total neutrino mass; $\sum m_\nu < 0.35$ eV at the 95% confidence level. Finally, we add the ‘‘Union 2.1 Compilation’’ supernovae data into the WMAP7+HST+SDSS+CFHTLS data combination and the constraint on the total neutrino mass becomes

$$\sum m_\nu < 0.33 \text{ eV} \quad (95\% \text{ C.L.}) . \quad (17)$$

We now present the constraints obtained from extending the ranges of multipoles to smaller scales; up to $\ell_{\max} = 960$.

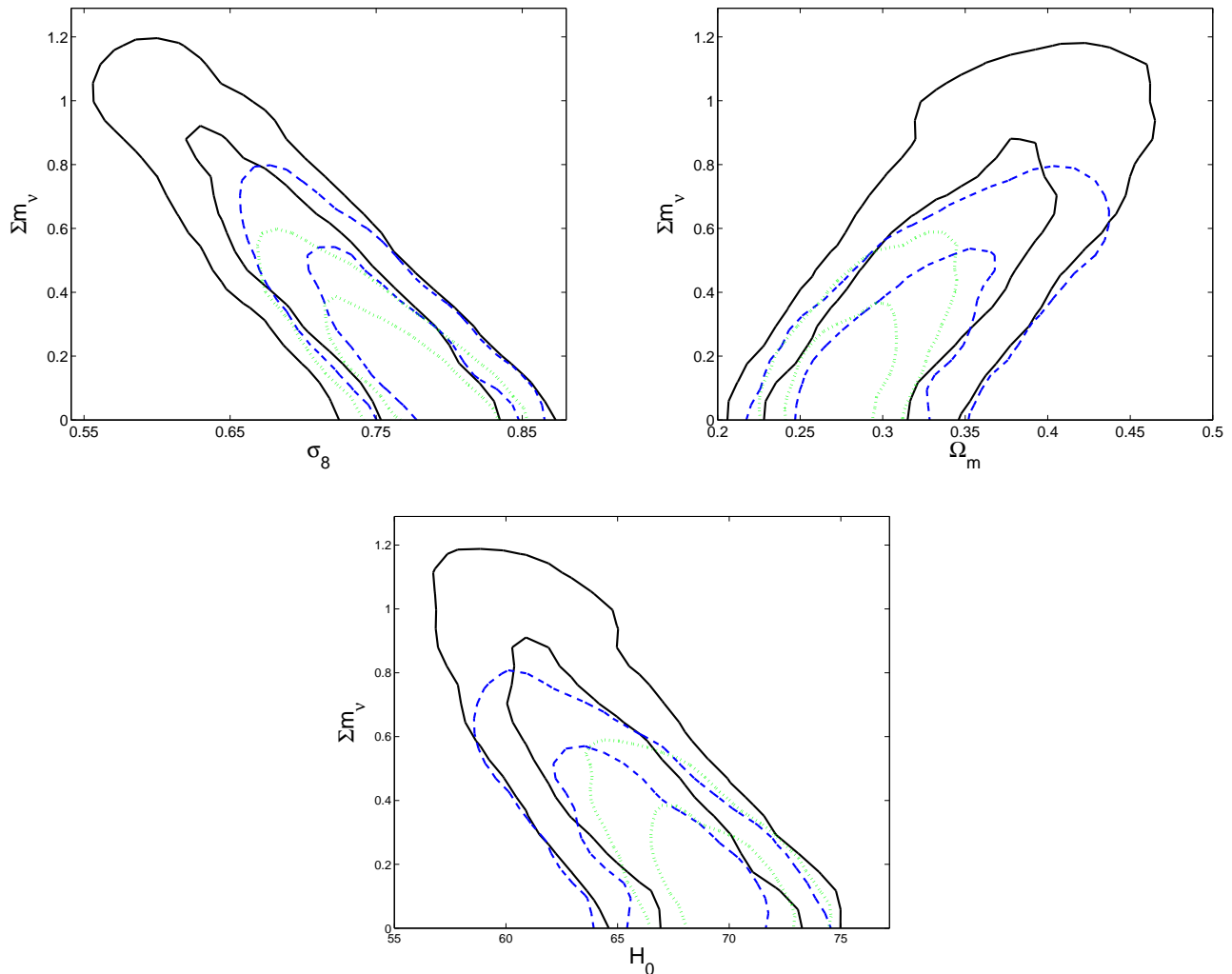


FIG. 5: Two-dimensional contours in the $(\sigma_8, \sum m_\nu)$, $(\Omega_m, \sum m_\nu)$ and $(H_0, \sum m_\nu)$ panels from different data combinations: WMAP7 alone (black solid lines), WMAP7+CFHTLS (blue dashed lines) and WMAP7+SDSS+CFHTLS (green dotted lines) for $\ell_{\max} = 630$.

The improvements from these scales are not negligible: if we consider CFHTLS data in combination with WMAP7 we go from $\sum m_\nu = 0.64$ eV to $\sum m_\nu < 0.43$ eV. If we also add the HST data we obtain $\sum m_\nu < 0.29$ eV, which has to be compared with the $\ell_{\max} = 630$ results of $\sum m_\nu = 0.41$ eV. Note that by adding SDSS and SN data the constraint improves and becomes $\sum m_\nu < 0.27$ eV at the 2σ C.L. level, which is the tightest bound on neutrinos presented in this paper.

It is evident that exploring the smaller scale matter power spectrum can significantly improve constraints obtained from larger scales. Our result above can be compared to the constraint obtained using only multipoles up to the linear theory value $\ell_{\max} = 150$, which is $\sum m_\nu < 0.43$ eV for the combined data set.

Finally, we have explored the effect that the error on the non-linear fitting formula for the matter power has on the final results. This error has been quantified in ref. [69], which presents an analytic expression, $E(k, z)$, the error on the suppression in the power spectrum due to neutrinos, which depends on scale, redshift and neutrino mass fraction, and is at the level of 5%. We computed the constraints by considering $P(k) = P(k)[1 + aE(k, z)]$, with a being a free parameter with standard deviation of unity. For all data sets the 2σ upper limit for $\ell_{\max} = 960$ weakens by only 0.01eV, demonstrating that the numerical errors for the scales considered here are smaller than statistical uncertainties on the data point and will not impact the final constraints. `Halofit` will also underestimate the matter power spectrum, in a manner independent of neutrino mass, by around 5% [75]. Neglecting this error, because it underestimates the matter power spectrum, is conservative and will only produce slightly weaker constraints. Furthermore, since the

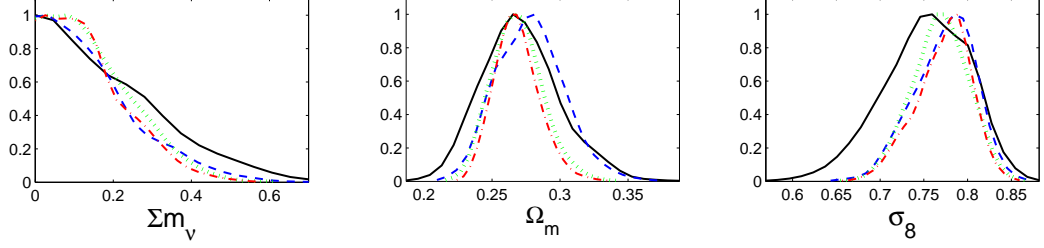


FIG. 6: One-dimensional marginalized likelihood constraints on the total neutrino mass Σm_ν , as well as other cosmological parameters, Ω_m and σ_8 from different data combinations: WMAP7+HST (black solid lines), WMAP7+HST+CFHTLS (blue dashed lines), WMAP7+HST+SDSS+CFHTLS (green dotted lines) and WMAP7+HST+SDSS+SN+CFHTLS (red dash-dot lines) for $\ell_{\max} = 630$.

magnitude of this error is similar to $E(k, z)$ and independent of neutrino mass, its effect should be small.

TABLE III: The 68% and 95% confidence levels on the effective number of neutrino species, N_{eff} from different data combinations.

Data sets	N_{eff}	
	$\ell_{\max} = 630$	$\ell_{\max} = 960$
WMAP7 alone	> 2.84 (95% C.L.)	
WMAP7 + SDSS	$4.13^{+1.20}_{-0.89}$ ($+4.05$, -2.00)	
WMAP7 + CFHTLS	$4.38^{+2.04}_{-1.16}$ ($+3.72$, -2.12)	$4.23^{+1.55}_{-0.70}$ ($+2.96$, -1.50)
WMAP7 + HST	$3.99^{+1.76}_{-0.41}$ ($+2.92$, -1.36)	
WMAP7 + HST + SDSS	$3.93^{+0.85}_{-0.73}$ ($+1.78$, -1.42)	
WMAP7 + HST + CFHTLS	$3.98^{+1.04}_{-0.51}$ ($+2.02$, -1.20)	$4.17^{+0.80}_{-0.67}$ ($+1.62$, -1.26)
WMAP7 + HST + SDSS + CFHTLS	$3.91^{+0.71}_{-0.68}$ ($+1.38$, -1.20)	$3.92^{+0.75}_{-0.51}$ ($+1.42$, -1.03)
WMAP7 + HST + SDSS + SN + CFHTLS	$3.92^{+0.61}_{-0.60}$ ($+1.33$, -1.17)	$3.91^{+0.67}_{-0.45}$ ($+1.26$, -0.96)

C. Relativistic Species N_{eff}

In this subsection, we consider the constraints on the effective number of neutrino species, N_{eff} , assuming massless neutrinos. Since N_{eff} can be written in terms of $\Omega_m h^2$ and the redshift of matter-radiation equality, z_{eq} , there are strong degeneracies present between N_{eff} , the matter density, $\Omega_m h^2$ and the Hubble parameter H_0 [5, 23]. CMB constraints on N_{eff} can thus be strongly improved by combining them with measurements of the small-scale matter power spectrum such as those obtained from SDSS or CFHTLS.

We find the WMAP7 data alone gives $N_{\text{eff}} > 2.84$ at the 95% confidence level, consistent with the result derived by the WMAP7 team [6]. Adding the CFHTLS data significantly improves the constraints on N_{eff} to

$$N_{\text{eff}} = 4.38^{+2.04}_{-1.16} \text{ } (^{+3.72}, ^{-2.12}) \quad (18)$$

at the 68% and 95% C.L. Figure 7 shows the two dimensional likelihood contours for both these constraints, with $\ell_{\max} = 630$, making it clear that the improvement is coming from degeneracy breaking. For comparison, when we use the SDSS DR4 LRG power spectra data instead of CFHTLS, we obtain the very consistent $N_{\text{eff}} = 4.13^{+1.20}_{-0.89}$ ($+4.05$, -2.00) (68 and 95% C.L.).

WMAP7+HST gives $N_{\text{eff}} = 3.99^{+1.76}_{-0.41}$ ($+2.92$, -1.36) (68 and 95% C.L.). Adding the CFHTLS angular power spectra tightens this to $N_{\text{eff}} = 3.98^{+1.04}_{-0.51}$ ($+2.02$, -1.20). This is similar to WMAP7+HST+SDSS, which gives $N_{\text{eff}} = 3.93^{+0.85}_{-0.73}$ ($+1.78$, -1.42). WMAP7+HST+SDSS+CFHTLS gives $N_{\text{eff}} = 3.91^{+0.71}_{-0.68}$ ($+1.38$, -1.20). Table III lists these constraints on N_{eff} , while figure 8 shows one-dimensional marginalized likelihood constraints on N_{eff} , $\Omega_m h^2$ and H_0 , with $\ell_{\max} = 630$.

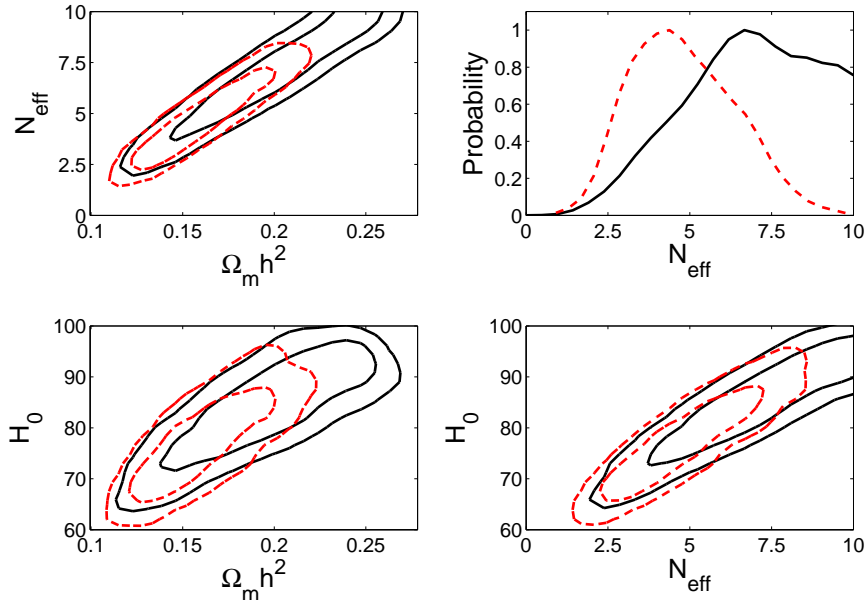


FIG. 7: Marginalized one-dimensional and two-dimensional likelihood ($1, 2\sigma$ contours) constraints on $\Omega_m h^2$, H_0 and N_{eff} from WMAP7 (black solid lines) and WMAP7+CFHTLS (red dashed lines) data combinations for $\ell_{\text{max}} = 630$.

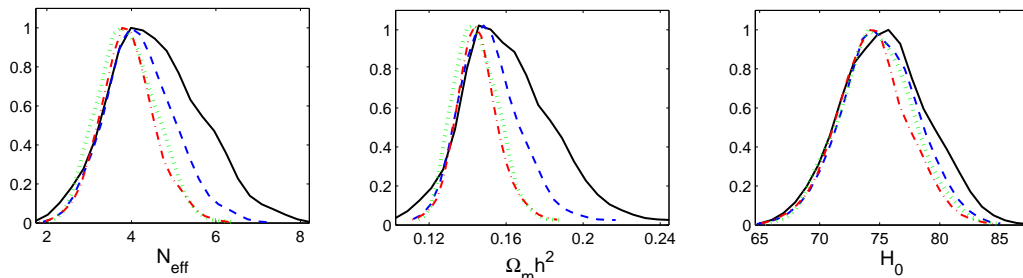


FIG. 8: One-dimensional marginalized likelihood constraints on N_{eff} , $\Omega_m h^2$ and H_0 from different data combinations: WMAP7+HST (black solid lines), WMAP7+HST+CFHTLS (blue dashed lines), WMAP7+HST+SDSS+CFHTLS (green dotted lines) and WMAP7+HST+SDSS+SN+CFHTLS (red dash-dot lines) for $\ell_{\text{max}} = 630$.

WMAP7+HST+SDSS+CFHTLS+SN gives our most stringent constraint of

$$N_{\text{eff}} = 3.92^{+0.61(+1.33)}_{-0.60(-1.17)} \quad (68\% \text{ and } 95\% \text{ C.L.}) . \quad (19)$$

We also consider the $\ell_{\text{max}} = 960$ case and find that the constraint improves slightly: $N_{\text{eff}} = 3.91^{+0.67(+1.26)}_{-0.45(-0.96)}$ for the 68% and 95% confidence levels. Our results are quite consistent with those of the ACT and SPT CMB experiments, which are $N_{\text{eff}} = 5.3 \pm 1.3$ and $N_{\text{eff}} = 3.85 \pm 0.62$ (68% confidence level), and, like them, display a slight preference for an extra relativistic relic [31, 32]. However, the standard value of $N_{\text{eff}} = 3.04$ remains well within the 95% confidence intervals.

VI. CONCLUSIONS AND DISCUSSIONS

Measurements of the galaxy power spectrum can put strong constraints on the neutrino mass and effective number of neutrino species. Significant gains can be made by probing weakly non-linear scales and investigating redshift

evolution. We have used the improved parametrization developed by ref. [69], who precisely calibrated the effect of massive neutrinos on the matter power spectrum using a suite of N-body simulations, to investigate non-linear scales.

Although the non-linear matter power spectrum may be estimated accurately from simulations, connecting it to the galaxy clustering is challenging. In this study, we have assumed a simple bias model with no dependence on scale. To check the validity of this model, we fit the power spectrum with a simple two-parameter Q bias model in Λ CDM without massive neutrinos. We find that the best-fitting Q model has negligible scale-dependence to $k \sim 0.6$ h/Mpc. We stress that this is only a consistency check, but it demonstrates that a scale-dependent bias model is not needed to fit the data at the redshifts we consider, $z > 0.5$, even to weakly non-linear scales of $k \sim 0.6$ h/Mpc. These results are in part due to the range of galaxy luminosities represented in the CFHTLS sample. The CFHTLS data set thus probes an interesting regime for neutrino studies for $z = 0.5 - 1.2$ at small scales that can be modeled with confidence.

We find that combining the CFHTLS data with WMAP already gives tight limits on the total neutrino mass. Adding additional low-redshift probes, including SDSS LRGs and SN, only marginally improves the constraints. We benefit considerably by extending the angular scale limit from $\ell_{\max} = 630$ to 960. This extends the fit from $k \sim 0.4$ h/Mpc to $k \sim 0.6$ h/Mpc. However, there is a strong correlation between galaxy bias and total neutrino mass, since both parameters modulate the amplitude of the galaxy power spectrum. Thus, future analyses can benefit from adding additional observables to constrain the galaxy bias.

We further constrain the effective number of neutrino species. Again, CFHTLS complements the WMAP7 data by constraining Ω_m leading to tighter limits on N_{eff} . We find that the constraining power of the CFHTLS data is similar to that of the SDSS LRG sample and the limits from both surveys are fully consistent.

The main constraints derived in this paper are summarized as follows: CFHTLS, combined with WMAP7 and a prior on the Hubble constant provides an upper limit of $\sum m_\nu < 0.29$ eV and $N_{\text{eff}} = 4.17_{-1.26}^{+1.62}$ (2σ confidence levels). If we instead omit smaller scales which may be affected by non-linearities, these constraints relax to the following values: $\sum m_\nu < 0.41$ eV and $N_{\text{eff}} = 3.98_{-1.20}^{+2.02}$ (2σ confidence levels). By combining with the SDSS LRG matter power and SN luminosity distance moduli we further improve to $\sum m_\nu < 0.27$ eV and $N_{\text{eff}} = 3.91_{-0.96}^{+1.26}$ (2σ confidence levels).

Acknowledgments

CFHTLS is based on observations obtained with MegaPrime/MegaCam, a joint project of CFHT and CEA/DAPNIA, at the Canada-France-Hawaii Telescope (CFHT) which is operated by the National Research Council (NRC) of Canada, the Institut National des Sciences de l'Univers of the Centre National de la Recherche Scientifique (CNRS) of France, and the University of Hawaii. This work is based in part on data products produced at TERAPIX and the Canadian Astronomy Data Centre as part of the Canada-France-Hawaii Telescope Legacy Survey, a collaborative project of NRC and CNRS.

We acknowledge the use of the Legacy Archive for Microwave Background Data Analysis (LAMBDA). Support for LAMBDA is provided by the NASA Office of Space Science. MV is supported by ASI/AAE, INFN/PD-51, PRIN MIUR, PRIN INAF 2009 and the European Research Council - Starting Grant "cosmoIGM". SPB is supported by NSF grant AST-0907969 and the Institute for Advanced Study. Funding for the SDSS and SDSS-II has been provided by the Alfred P. Sloan Foundation, the Participating Institutions, the National Science Foundation, the U.S. Department of Energy, the National Aeronautics and Space Administration, the Japanese Monbukagakusho, the Max Planck Society, and the Higher Education Funding Council for England. The SDSS Web Site is <http://www.sdss.org/>. The SDSS is managed by the Astrophysical Research Consortium for the Participating Institutions. The Participating Institutions are the American Museum of Natural History, Astrophysical Institute Potsdam, University of Basel, University of Cambridge, Case Western Reserve University, University of Chicago, Drexel University, Fermilab, the Institute for Advanced Study, the Japan Participation Group, Johns Hopkins University, the Joint Institute for Nuclear Astrophysics, the Kavli Institute for Particle Astrophysics and Cosmology, the Korean Scientist Group, the Chinese Academy of Sciences (LAMOST), Los Alamos National Laboratory, the Max-Planck-Institute for Astronomy (MPIA), the Max-Planck-Institute for Astrophysics (MPA), New Mexico State University, Ohio State University, University of Pittsburgh, University of Portsmouth, Princeton University, the United States Naval Observatory, and the University of Washington.

-
- [1] A. D. Dolgov, Phys. Rept. **370**, 333 (2002).
 - [2] J. Lesgourgues and S. Pastor, Phys. Rept. **429**, 307 (2006).
 - [3] D. N. Spergel *et al.*, Astrophys. J. Suppl. **148**, 175 (2003).

- [4] D. N. Spergel *et al.*, *Astrophys. J. Suppl.* **170**, 377 (2007).
- [5] E. Komatsu *et al.*, *Astrophys. J. Suppl.* **180**, 330 (2009).
- [6] E. Komatsu *et al.*, *Astrophys. J. Suppl.* **192**, 18 (2011).
- [7] W. Hu, D. J. Eisenstein and M. Tegmark, *Phys. Rev. Lett.* **80**, 5255 (1998).
- [8] Ø. Elgarøy *et al.*, *Phys. Rev. Lett.* **89**, 061301 (2002).
- [9] S. W. Allen, R. W. Schmidt and S. L. Bridle, *Mon. Not. Roy. Astron. Soc.* **346**, 593 (2003).
- [10] V. Barger, D. Marfatia and A. Tregre, *Phys. Lett.* **B595**, 55 (2004).
- [11] S. Hannestad, *JCAP* **0305**, 004 (2003).
- [12] M. Tegmark *et al.*, *Phys. Rev.* **D69**, 103501 (2004).
- [13] S. Hannestad and G. Raffelt, *JCAP* **0404**, 008 (2004).
- [14] P. Crotty, J. Lesgourgues and S. Pastor, *Phys. Rev.* **D69**, 123007 (2004).
- [15] Ø. Elgarøy and O. Lahav, *New J. Phys.* **7**, 61 (2005).
- [16] S. Hannestad, *Phys. Rev. Lett.* **95**, 221301 (2005).
- [17] G. L. Fogli *et al.*, *Phys. Rev.* **D78**, 033010 (2008).
- [18] J.-Q. Xia, H. Li, G.-B. Zhao and X. Zhang, *Phys. Rev.* **D78**, 083524 (2008).
- [19] S. A. Thomas, F. B. Abdalla and O. Lahav, *Phys. Rev. Lett.* **105**, 031301 (2010).
- [20] T. Sekiguchi, K. Ichikawa, T. Takahashi and L. Greenhill, *JCAP* **1003**, 015 (2010).
- [21] B. Reid *et al.*, *Mon. Not. Roy. Astron. Soc.* **404**, 60 (2010).
- [22] B. Reid *et al.*, *Mon. Not. Roy. Astron. Soc.* **401**, 2148 (2010).
- [23] B. Reid, L. Verde, R. Jimenez and O. Mena, *JCAP* **1001**, 003 (2010).
- [24] S. Saito, M. Takada and A. Taruya, *Phys. Rev.* **D83**, 043529 (2011).
- [25] S. Riemer-Sørensen *et al.*, arXiv:1112.4940.
- [26] U. Seljak *et al.*, *Phys. Rev.* **D71**, 103515 (2005).
- [27] A. Goobar, S. Hannestad, E. Mörtzell and H. Tu, *JCAP* **0606**, 019 (2006).
- [28] U. Seljak, A. Slosar and P. McDonald, *JCAP* **0610**, 014 (2006).
- [29] S. Ho *et al.*, arXiv:1201.2137
- [30] R. De Putter *et al.*, arXiv:1201.1909
- [31] J. Dunkley *et al.*, *Astrophys. J.* **739**, 52 (2011).
- [32] R. Keiser *et al.*, *Astrophys. J.* **743**, 28 (2011).
- [33] J. Dunkley *et al.*, *Astrophys. J. Suppl.* **180**, 306 (2009).
- [34] K. Ichikawa, M. Kawasaki and F. Takahashi, *JCAP* **0705**, 007 (2007).
- [35] G. Mangano *et al.*, *JCAP* **0703**, 006 (2007).
- [36] J. Hamann, S. Hannestad, G. G. Raffelt and Y. Y. Y. Wong, *JCAP* **0708**, 021 (2007).
- [37] A. Mantz, S. W. Allen and D. Rapetti, *Mon. Not. Roy. Astron. Soc.* **406**, 1805 (2010).
- [38] Y. Goranova *et al.*, The CFHTLS T0006 Release, <http://terapix.iap.fr/cplt/T0006-doc.pdf>, (2009).
- [39] L. Fu *et al.*, *Astron. Astrophys.* **479**, 9 (2008).
- [40] H. Li *et al.*, *Phys. Lett.* **B675**, 164 (2009).
- [41] M. Kilbinger *et al.*, *Astron. Astrophys.* **497**, 677 (2009).
- [42] H. Shan *et al.*, arXiv:1108.1981.
- [43] I. Tereno *et al.*, *Astron. Astrophys.* **500**, 657 (2009).
- [44] J. Coupon *et al.*, arXiv:1107.0616.
- [45] B. R. Granett *et al.*, *Mon. Not. Roy. Astron. Soc.* **421**, 251 (2012).
- [46] R. E. Smith, R. Scoccimarro and R. K. Sheth, *Phys. Rev.* **D75**, 063512 (2007).
- [47] J. G. Cresswell and W. J. Percival, *Mon. Not. Roy. Astron. Soc.* **392**, 682 (2009).
- [48] W. J. Percival *et al.*, *Astrophys. J.* **657**, 645 (2007).
- [49] P. Schneider, *Astrophys. J.* **498**, 43 (1998).
- [50] N. Hamaus, U. Seljak, V. Desjacques, R. E. Smith and T. Baldauf, *Phys. Rev.* **D82**, 043515 (2010).
- [51] M. E. C. Swanson, W. J. Percival, & O. Lahav, *Mon. Not. Roy. Astron. Soc.* **409**, 1100 (2010).
- [52] J. Coupon *et al.*, *Astron. Astrophys.* **500**, 981 (2009).
- [53] I. Zehavi *et al.*, *Astrophys. J.* **736**, 59 (2011).
- [54] W. J. Percival, L. Verde and J. A. Peacock, *Mon. Not. Roy. Astron. Soc.* **347**, 645 (2004).
- [55] N. Padmanabhan *et al.*, *Mon. Not. Roy. Astron. Soc.* **378**, 852 (2007).
- [56] L. Guzzo *et al.*, in preparation.
- [57] M. Tegmark, *Phys. Rev.* **D55**, 5895 (1997).
- [58] J. R. Bond, A. H. Jaffe and L. Knox, *Phys. Rev.* **D57**, 2117 (1998).
- [59] D. Huterer, L. Knox and R. C. Nichol, *Astrophys. J.* **555**, 547 (2001).
- [60] M. Tegmark *et al.*, *Astrophys. J.* **571**, 191 (2002).
- [61] K. M. Górski *et al.*, *Astrophys. J.* **622**, 759 (2005).
- [62] M. Tegmark *et al.*, *Phys. Rev.* **D69**, 103501 (2006).
- [63] A. G. Riess *et al.*, *Astrophys. J.* **699**, 539 (2009).
- [64] W. L. Freedman *et al.*, *Astrophys. J.* **553**, 47 (2001).
- [65] N. Suzuki *et al.*, *Astrophys. J.* **746**, 85 (2012).
- [66] M. Goliath, R. Amanullah, P. Astier, A. Goobar and R. Pain, *Astron. Astrophys.* **380**, 1 (2001).
- [67] E. Di Pietro and J. F. Claeskens, *Mon. Not. Roy. Astron. Soc.* **341**, 1299 (2003).

- [68] R. E. Smith *et al.*, Mon. Not. Roy. Astron. Soc. **341**, 1311 (2003).
- [69] S. Bird, M. Viel and M. G. Haehnelt, Mon. Not. Roy. Astron. Soc. **420**, 2551 (2012).
- [70] M. Viel, M. G. Haehnelt and V. Springel, JCAP **1006**, 015 (2010).
- [71] F. Marulli *et al.*, Mon. Not. Roy. Astron. Soc. **364**, 418 (2011).
- [72] A. Lewis and S. Bridle, Phys. Rev. **D66**, 103511 (2002); URL: <http://cosmologist.info/cosmomc/>.
- [73] S. Hannestad and G. G. Raffelt, JCAP **0611**, 016 (2006).
- [74] S. Cole *et al.*, Mon. Not. Roy. Astron. Soc. **362**, 505 (2005).
- [75] K. Heitmann *et al.*, Astrophys. J. **715**, 104 (2010).